The Deep Roots of Geology: Tectonic History of Australia Preserved as Mantle Anisotropy

Caroline M. Eakin[1*]

[1]*Research School of Earth Sciences, Australian National University, Canberra, Australia*

Australia is an old stable continent with a rich geological history. Limitations in sub-surface imaging below the Moho, however, mean that is unclear to what extent, and to what depth, this rich geological history is expressed in the mantle. Scattering of surface waves at ~150km depth by lateral gradients or boundaries in seismic anisotropy, termed Quasi-Love waves, offer potential new insights. The first such analysis for Australia and Zealandia shown here detects over 300 new scatterers that display striking geographical patterns. Around two-thirds of the scatterers are coincident with either the continental margins, or major crustal boundaries within Australia, suggesting deep mantle roots to such features. Within the continental interior such lateral anisotropic gradients imply pervasive fossilized lithospheric anisotropy, on a scale that mirrors the crustal geology at the surface, and a strong lithosphere that preserves this signal over billions of years. Along the continental margins, lateral anisotropic gradients may indicate either the edge of the thick continental lithosphere, or small-scale dynamic processes in the asthenosphere, such as edge-drive convection, tied to the transition from oceanic to continental crust/lithosphere.

The Australian continent preserves a vast tectonic history, stretching from the Archean to the present day. By the Neoproterozoic, supercontinent cycles had assembled the Australian cratons, while later continental accretion added the eastern orogens in the Phanerozoic. Since the break-up of eastern Gondwana, and the formation of its rifted passive margins, the Australian continent has moved northwards colliding with SE Asia. Today, Australia is the fastest moving continent on Earth, exerting significant shear on the underlying mantle asthenosphere. Such deformation is thought to cause a lattice preferred orientation (LPO) in olivine generating strong azimuthal anisotropy aligned with plate motion [1,2]. Intriguingly, this strong azimuthal anisotropy is not detected by shear-wave splitting studies, with weak and complex splitting generally observed across Australia [3–5]. Instead a contrasting contribution from fossilized anisotropy in the lithosphere has been proposed, frozen-in by past deformational events [4,6].

Observations of scattered surface waves, termed Quasi-Love (QL) waves [7], can be used to pinpoint the location of lateral gradients in seismic anisotropy in the upper mantle (Fig. 1), such as those that may exist along present (and/or past) plate boundaries. When a Love wave encounters such a boundary, a portion of its energy is scattered from Love into Rayleigh wave motion, generating a QL wave (Fig. 1). The QL wave retains a similar waveform shape as the fundamental Love wave (G1), hence 'Quasi-Love', but travels with the slower velocity of the fundamental Rayleigh wave (R1). This principle can be exploited to determine the distance (δx) the QL wave has travelled and thus pinpoint the location of the anisotropic gradient. Previously QL waves have been detected across a wide range of tectonic settings from continental collision [8,9], seafloor spreading [10], subduction [7,11–13], and hotspot volcanism [14,15]. Most recently QL waves have been recorded along the continental margin of eastern North America [16], implying localized dynamic processes and a disruption of the underlying mantle flow-field at the margin, potentially

induced by the transition from continental to oceanic lithosphere. As of yet, however, there have been no such studies targeting the rich history of the Australian continent and its extensive passive margins.

Results

Using seismic stations from the Australian National Seismograph Network, and shallow earthquakes at 70°-180° epicentral distance, QL waves were detected on 23% of the 2364 available event-station pairs (Fig. 2, Supplementary Data Table S1) with 303 QL scatterers falling within the study area, as shown in Fig. 3. The QL waves detected are of varying amplitude (represented by their symbol size) which is a function of the strength of the anisotropic gradient as well as the geometry of the anisotropy relative to the angle of the raypath. The back-projected scatterers are widely distributed, comprising one of the largest and most geographically diverse QL datasets produced to date, as well as the first results within Australasia. While the QL scatterers are widespread and numerous (the reliability of any single measurement should be treated with caution), when considered collectively, they display a striking correspondence with many tectonic and crustal features at the Earth's surface (Fig. 3 and Figs. S4-7). Most noteworthy are continental margins (blue circles; Fig. 3a-b) with almost one-third of scatterers (96; 32%) falling within 1° of the continental margin, i.e. the boundary between continental and oceanic crust [17]. The pattern is particularly remarkable around the Tasman Sea, along the former rift boundary between Australia and Zealandia (Fig. 3b). The scatterers appear to closely follow curvatures in this boundary and even coincide with micro-continents such as the East Tasman Plateau (ETP) and Gilbert Seamount Complex (GSC), which were isolated from the mainland during the rifting process [18].

Intriguingly, a considerable number of scatterers also fall within the Australian continental interior, and most coincide with major tectonic provinces (yellow circles; Fig. 3). In total, 83 scatterers lie within 1° of a known major crustal boundary in Australia (dotted yellow lines)[19]. These crustal boundaries, mapped from the accumulation of 30 years worth of deep seismic, geological and geophysical data, reflect ancient plate boundaries where individual crustal blocks have been assembled together forming the internal architecture of the continent. Similarly, many of these features are associated with prominent gravity anomalies (Fig. 3c), indicating that they represent major crustal structures. Scatterers can often be found on the edge of these strong anomalies, such as the east-west trending Musgrave and Arunta blocks in central Australia, and the north-south trending Darling Fault in Western Australia at the southwest corner of the Yilgarn Craton. Within the submerged continental area of Zealandia a correspondence with topographic variations at the surface can also be seen (Fig. 3a), particularly near New Caledonia (NC) and along the New Caledonia Trough and Norfolk Ridge. This hints at an association with the internal geological architecture of Zealandia similar to that within Australia.

Numerous scatterers can also be found in the oceans, in particular in the middle of the Tasman Sea (between Australia and Zealandia) where scatterers appear to be associated with the Tasman spreading ridge, an extinct mid-ocean ridge where spreading ceased 52 Myr ago [20]. As well as ancient tectonic features, multiple scatterers can be found at present day plate boundaries (white dashed lines and white circles; Fig. 3), such as the New Hebrides Trench (NHT).

Discussion

The results of this study reveal the widespread presence of lateral anisotropic gradients capable of generating QL waves. The location of such gradients appear closely linked to tectonic boundaries and major crustal features visible from the Earth's surface, which by inference, must also extend to depth within the mantle. With a dominant frequency of 0.01Hz (100s) the QL wave has peak sensitivity between 100-200km depth [8,12], well below even the thickest continental crust. For central and western Australia this depth range would sample the old thick cratonic lithosphere (blue colors; Fig. 4b-c), while for eastern Australia the lithosphere is younger (Phanerozoic) and much thinner, ~75km [21]. Except in regions of thick continental lithosphere, the QL scatterers should therefore correspond to lateral anisotropic gradients in the asthenosphere, where olivine LPO is expected to develop through mantle flow [22].

A large number of scatterers in our dataset are associated with continental margins (Fig. 3a-b), similar to the findings of Servali et al., (2020) who detected pervasive scatterers along the eastern North America passive margin. For western and southern Australia the margin is co-located with the edge of the thick continental lithosphere (Fig. 4). QL scatterers along this boundary may therefore simply reflect the transition from active flow in the asthenosphere to anisotropy fossilized within the lithosphere. Alternatively a significant step in lithospheric thickness may trigger edge-driven convection (EDC) at the margin [23]. Numerous scatterers along the eastern margin of Australia, and the western margin of Zealandia, are however less easy to explain given that there is little apparent variation in lithospheric thickness. This may instead hint at a fundamental difference between how continental versus oceanic lithosphere couples to the underlying asthenosphere, perhaps in terms of differences in viscosity [24]. Alternatively finer-scale variations in lithospheric thickness along the margins may exist than those currently resolved. Such 3D topography on the lithosphere-asthenosphere boundary may locally divert or

disrupt the mantle flow-field, such as localized EDC processes proposed at the Newer Volcanics Province in SE Australia [25,26].

Another significant finding of this study is the presence of numerous QL scatterers associated with major crustal boundaries within Australia (Fig. 3). Most of these scatterers are located within thick Precambrian cratonic lithosphere (Fig. 4), implying scatterers originate due to anisotropy frozen-in since the last deformational episode, and therefore that they record the evolution of the continent. Furthermore this implies that geological boundaries are preserved over billions of years not only in the crust but also as anisotropic boundaries at significant depth (>100km) in the lithospheric mantle. If fossilized lithospheric anisotropy is pervasive, yet heterogenous with strong lateral gradients, this lithospheric layer would add interference to the SKS splitting accrued from the strong active flow in the underlying mantle, causing a loss of coherency in the overall signal. This may explain the long-standing conundrum as to why SKS splitting is perplexingly weak and complex across Australia [3–5], despite fast Australian plate motion, and strong azimuthal anisotropy imaged beneath the continent (Fig. 4c) [1,2,6]. Further studies to constrain lithospheric anisotropy may therefore help to decode the complex SKS splitting, as well as provide further insights on the past deformational history of continent.

Conclusion

Observations of QL waves have revealed extensive lateral anisotropic gradients beneath the Australian continent, preserving a rich and ancient tectonic history as fossilized lithospheric anisotropy. Small-scale convective processes in the asthenosphere, such as EDC, likely also play a role in generating scatterers, particularly along the continental margins of the Tasman Sea where the lithosphere is younger and thinner. In the future QL scatterers may be used as a

predictive tool, helping to constrain major crustal structures at depth, such as those currently hidden under cover [19], and in particular identifying those with deep mantle connections that may suggest potential for mineralization [27,28].

Methods

Overview of data selection and processing

Earthquakes from 1994-2020 of magnitude >6.5, depth <100 km, and in the epicentral distance range of 70°-180° were selected to ensure large amplitude surface waves and enough separation to distinguish QL from R1. All data are low-pass filtered at 100s (0.01Hz) to isolate the fundamental Love and Rayleigh wave components and suppress overtones. At low frequencies the surface waves are insensitive to shallow crustal structure, with peak sensitivity in the mantle between 100-200km depth (refer to Fig. S1 of Levin et al. (2007), Fig. 9 of Chen and Park (2013)). Following previous studies, the delay time (δt) between the QL and G1 is calculated using the cross-correlation technique [8,10,16]. In the final step the delay time is converted to distance (see Fig. 1b), and back-projected along the great-circle path to determine the location of the scatterer. In this study a few modifications have been made to the cross-correlation technique to improve detection and measurement quality. These are outlined in further detail below along with a more detailed description of the methodology.

Strategy for Detection and Measurement of Quasi-Love Waves

Data for each event is requested from the IRIS Data Management Centre (ds.iris.edu/) for 5000 seconds following the origin time. After low-pass filtering at 0.01Hz, seismograms are rotated into the vertical, radial, and transverse, and normalised by the maximum amplitude on each

component. The maximum on the transverse signifies the fundamental Love wave (G1), and on the vertical the fundamental Rayleigh wave (R1), indicated by the vertical dashed green and dashed blue lines in Fig. S1. Initial quality control restricts events to those with a signal-to-noise ratio (SNR) of the Love wave greater than 5, where the 'noise' amplitude is determined by the first 300 seconds of the seismogram. A cut-off of 5 was determined empirically from the data. In general large amplitude Love waves are a necessary pre-requirement to generating observable QL waves, given that gradients of 3-5% anisotropy will produce QL amplitudes of 5-10% of the Love wave [9].

Most previous studies only measure QL waves on the vertical component even though the particle motion is elliptical and distributed across both the vertical and radial components (Fig. S1b-c). Same as for R1, for QL, the vertical and radial components are 90° out of phase. The first derivative of the radial component (dashed red line Fig. S1d) matches the vertical component. This is a useful diagnostic feature. Any seismograms that do not display this characteristic during the visual inspection process are discarded, and the QL wave must be clearly visible on both components, not just the vertical. Furthermore, stacking of the vertical component with the derivative of the radial component amplifies the QL (and R1) while dampening the noise (magenta line Fig. S1e). This improves both the visibility and confidence of the QL detection.

The next step is to cross-correlate this QL stack with G1 on the transverse component. Fig. S1f shows the absolute amplitude of the cross-correlation (thin black line) as a function of lag time relative to the position of G1. Peaks of this cross-correlation function (i.e. maxima, where the

derivative equals zero) are identified by blue crosses and connected by a new blue curve. Peaks in this new curve are then selected and highlighted by blue circles. Typically the largest peak is associated with the correlation between G1 and R1 (as seen in Fig. S1f). The QL peak, if present, is a secondary peak located before the highest R1 peak but after the G1 arrival (indicated by dashed green line). The inferred QL delay time is marked by a green asterisk and dotted green line. The time shifted Love wave is plotted for comparison with the QL stack in Fig. S1e.

All seismograms and cross-correlation functions are visually inspected for quality based on the criteria outlined above. Only those with a clearly visible and distinct QL wave are kept. It is possible however that multiple QL waveforms may appear in one seismogram if multiple scatterers are located along the great circle path. In such cases, for simplicity, the first QL wave, closest to G1, and therefore closest to Australia is recorded. Conversely, the absence of a QL detection (Fig. S3) is not necessarily evidence for an absence of scatterers. QL amplitude is dependent not only on the strength of the anisotropic gradient but also on the anisotropic geometry relative to the propagation path. Maximum QL conversion will occur when the propagation azimuth is 45° to the symmetry axis, and zero conversion when the propagation azimuth is either parallel or perpendicular [10,29]. This creates a symmetric four-lobed radiation pattern with both positive and negative polarities of the QL wave, which in theory could be used to infer not only the location of an anisotropic gradient but also the geometry of anisotropy. The amplitude of the QL wave will therefore also vary as a function of propagation azimuth, as well as the strength of the anisotropic gradient. A particularly large QL amplitude is therefore indicative of the presence of a strong gradient but a small amplitude, or even absence of a QL wave, is not conclusive evidence of a weak or non-existent gradient.

The last step in the process is to convert the delay time (δt) into distance and back-project the location of the scatterer along the great-circle path. Considering that the QL wave travels distance, δx, of the total path, Δ, (Fig. 1a) with the slower Rayleigh wave phase velocity (V_R), the delay time can be expressed as:

$$\delta t = \frac{\delta x}{V_R} - \frac{\delta x}{V_L} \quad (1)$$

Where V_L is the Love wave phase velocity. To negate having to use either an average guess for the phase velocities or calculate individually for every seismogram, the following substitution can be made,

$$\delta t = \frac{\delta x (t_R - t_L)}{\Delta} \quad (2)$$

where Δ is the epicentral distance between source and receiver, and $t_R - t_L$ is the time delay between the Rayleigh (R1) and Love (G1) waves. Simply rearranging this equation for δx gives,

$$\delta x = \frac{\delta t \, \Delta}{(t_R - t_L)} \quad (3)$$

The scatterer distance is therefore independent of the absolute phase velocities or the arrival times, and only depends on the relative time difference between G1 and R1. This is useful given the exact start of the R1 is difficult to determine, especially considering likely overlap with QL. Instead the time difference between the maximum amplitude of G1 and R1 can be utilized, which is much easier to calculate from the seismogram.

Acknowledgements

Figures were made using Generic Mapping Tools [30], GeoMapApp (www.geomapapp.org), and AUSGIN (portal.geoscience.gov.au). Seismic data from the Australian National Seismograph Network (network AU; www.fdsn.org/networks/detail/AU/) were obtained via the Data Management Center of Incorporated Research Institutions for Seismology (ds.iris.edu/). This work was supported by grant DE190100062 from the Australian Research Council.

References

1. Debayle, E., Kennett, B. & Priestley, K. Global azimuthal seismic anisotropy and the unique plate-motion deformation of Australia. *Nature* **433**, 509–512 (2005).
2. Debayle, E., Dubuffet, F. & Durand, S. An automatically updated S -wave model of the upper mantle and the depth extent of azimuthal anisotropy. *Geophys. Res. Lett.* **43**, 674–682 (2016).
3. Heintz, M. & Kennett, B. L. N. Continental scale shear wave splitting analysis: Investigation of seismic anisotropy underneath the Australian continent. *Earth Planet. Sci. Lett.* **236**, 106–119 (2005).
4. Heintz, M. & Kennett, B. L. N. The apparently isotropic Australian upper mantle. *Geophys. Res. Lett.* **33**, L15319 (2006).
5. Bello, M., Cornwell, D. G., Rawlinson, N. & Reading, A. M. Insights into the structure and dynamics of the upper mantle beneath Bass Strait, southeast Australia, using shear wave splitting. *Phys. Earth Planet. Inter.* **289**, 45–62 (2019).
6. Yoshizawa, K. & Kennett, B. L. N. The lithosphere-asthenosphere transition and radial anisotropy beneath the Australian continent. *Geophys. Res. Lett.* **42**, 3839–3846 (2015).

7. Park, J. & Yu, Y. Seismic Determination of Elastic Anisotropy and Mantle Flow. *Science (80-.).* **261**, 1159–1162 (1993).
8. Chen, X. & Park, J. Anisotropy gradients from QL surface waves: Evidence for vertically coherent deformation in the Tibet region. *Tectonophysics* **608**, 346–355 (2013).
9. Yu, Y., Park, J. & Wu, F. Mantle anisotropy beneath the Tibetan Plateau: evidence from long-period surface waves. *Phys. Earth Planet. Inter.* **87**, 231–246 (1995).
10. Rieger, D. M. & Park, J. USArray observations of quasi-Love surface wave scattering: Orienting anisotropy in the Cascadia plate boundary. *J. Geophys. Res.* **115**, B05306 (2010).
11. Kobayashi, R. & Nakanishi, I. Location of Love-to-Rayleigh conversion due to lateral heterogeneity or azimuthal anisotropy in the upper mantle. *Geophys. Res. Lett.* **25**, 1067–1070 (1998).
12. Levin, V., Park, J., Lucente, F. P., Margheriti, L. & Pondrelli, S. End of subduction in northern Apennines confirmed by observations of quasi-Love waves from the great 2004 Sumatra-Andaman earthquake. *Geophys. Res. Lett.* **34**, 1–5 (2007).
13. Margheriti, L. *et al.* Large-scale coherent anisotropy of upper mantle beneath the Italian peninsula comparing quasi-Love waves and SKS splitting. *J. Geodyn.* **82**, 26–38 (2014).
14. Levin, V. & Park, J. Quasi-Love phases between Tonga and Hawaii: Observations, simulations, and explanations. *J. Geophys. Res. Solid Earth* **103**, 24321–24331 (1998).
15. Yu, Y. & Park, J. Hunting for azimuthal anisotropy beneath the Pacific Ocean region. *J. Geophys. Res.* **99**, 15399 (1994).
16. Servali, A., Long, M. D., Park, J., Benoit, M. H. & Aragon, J. C. Love-to-Rayleigh scattering across the eastern North American passive margin. *Tectonophysics* 228321

(2020). doi:10.1016/J.TECTO.2020.228321

17. Müller, R., Sdrolias, M., Gaina, C. & Roest, W. Age, spreading rates, and spreading asymmetry of the world's ocean crust. *Geochemistry, Geophys. Geosystems* **9**, 18–36 (2008).

18. Gaina, C., Müller, R. D., Brown, B. & Ishihara, T. Micro-continent formation around Australia. in *The Evolution and Dynamics of the Australian Plate* (eds. Hillis, R. & Müller, R. D.) 405–416 (Geological Society of Australia, 2003).

19. Korsch, R. J. & Doublier, M. P. Major crustal boundaries of Australia. (2015). doi:10.4225/25/555C181CC0EAE

20. Gaina, C. *et al.* The tectonic history of the Tasman Sea: A puzzle with 13 pieces. *J. Geophys. Res. Solid Earth* **103**, 12413–12433 (1998).

21. Kennett, B. L. N. & Salmon, M. AuSREM: Australian Seismological Reference Model. *Aust. J. Earth Sci.* **59**, 1091–1103 (2012).

22. Nicolas, A. & Christensen, N. I. Formation of anisotropy in upper mantle peridotites: A review. in *Composition, structure and dynamics of the lithosphere-asthenosphere system* 111–123 (American Geophysical Union, 1987). doi:10.1029/GD016p0111

23. King, S. D. & Anderson, D. L. Edge-driven convection. *Earth Planet. Sci. Lett.* **160**, 289–296 (1998).

24. Conrad, C. P., Behn, M. D. & Silver, P. G. Global mantle flow and the development of seismic anisotropy: Differences between the oceanic and continental upper mantle. *J. Geophys. Res.* **112**, (2007).

25. Davies, D. R. & Rawlinson, N. On the origin of recent intraplate volcanism in Australia. *Geology* **42**, 1031–1034 (2014).

26. Rawlinson, N., Davies, D. R. & Pilia, S. The mechanisms underpinning Cenozoic intraplate volcanism in eastern Australia: Insights from seismic tomography and geodynamic modeling. *Geophys. Res. Lett.* **44**, 9681–9690 (2017).

27. Hronsky, J. M. A., Groves, D. I., Loucks, R. R. & Begg, G. C. A unified model for gold mineralisation in accretionary orogens and implications for regional-scale exploration targeting methods. *Miner. Depos.* **47**, 339–358 (2012).

28. Hoggard, M. J. *et al.* Global distribution of sediment-hosted metals controlled by craton edge stability. *Nat. Geosci.* **13**, 504–510 (2020).

29. Park, J. Free oscillations in an anisotropic earth: path-integral asymptotics. *Geophys. J. Int.* **129**, 399–411 (1997).

30. Wessel, P., Smith, W. H. F., Scharroo, R., Luis, J. & Wobbe, F. Generic Mapping Tools: Improved Version Released. *Eos, Trans. Am. Geophys. Union* **94**, 409–410 (2013).

31. Bird, P. An updated digital model of plate boundaries. *Geochemistry, Geophys. Geosystems* **4**, (2003).

32. Amante, C. & Eakins, B. W. ETOPO1 1 arc-minute global relief model: procedures, data sources and analysis. *NOAA Tech. Memo. NESDIS NGDC-24* 19 (2009).

33. Sandwell, D. T., Müller, R. D., Smith, W. H. F., Garcia, E. & Francis, R. New global marine gravity model from CryoSat-2 and Jason-1 reveals buried tectonic structure. *Science (80-.).* **346**, 65–67 (2014).

34. Raymond, O. L., Totterdell, J. M., Woods, M. A. & Stewart, A. J. Australian Geological Provinces 2018.01 edition. (2018). doi:http://pid.geoscience.gov.au/dataset/ga/116823

35. Schaeffer, A. J. & Lebedev, S. Global shear speed structure of the upper mantle and transition zone. *Geophys. J. Int.* **194**, 417–449 (2013).

Figures

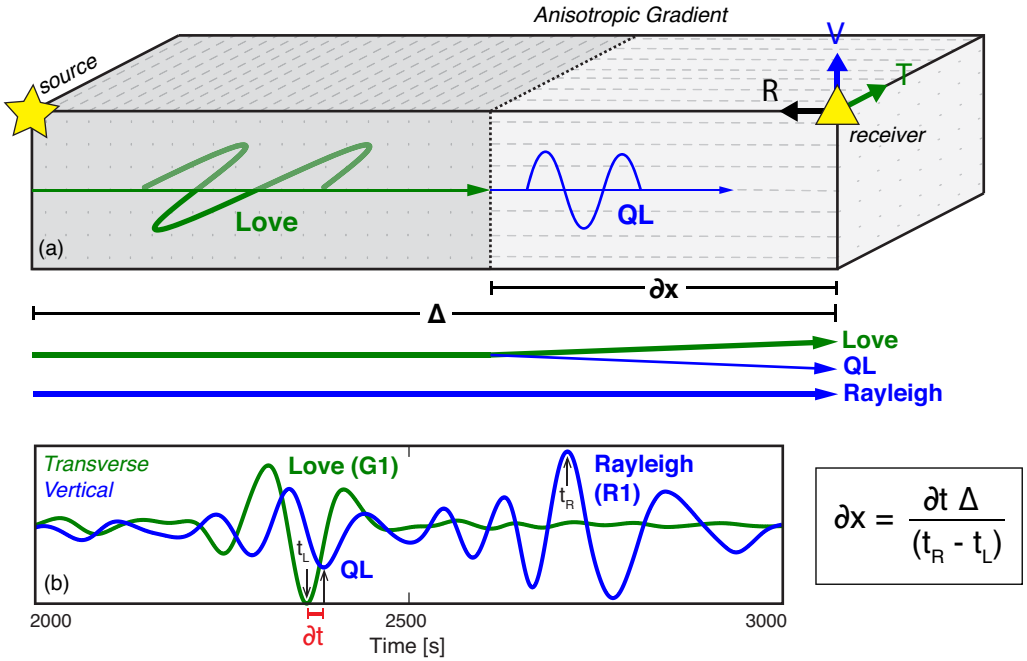

Figure 1. Process of QL wave scattering due to an anisotropic gradient. (a): Schematic illustration of a Love wave with transverse (T) particle motion (indicated in green), which upon encountering a lateral gradient in seismic anisotropy, partially converts into a QL wave with the same phase velocity and vertical (V) particle motion (indicated by blue) as a Rayleigh wave. The fundamental Love (G1) and Rayleigh (R1) waves travel a distance Δ between the source and receiver, whereas the QL wave only travels a distance δx between the scattering point and the receiver. The scattering is caused by a change in strength and/or orientation of the mantle anisotropy, indicated by the grey fabric pattern. (b): Example recording of a prominent QL wave arrival. The distance to the scattering point (δx) is related to the time delay (δt) between the QL and G1 via the equation shown.

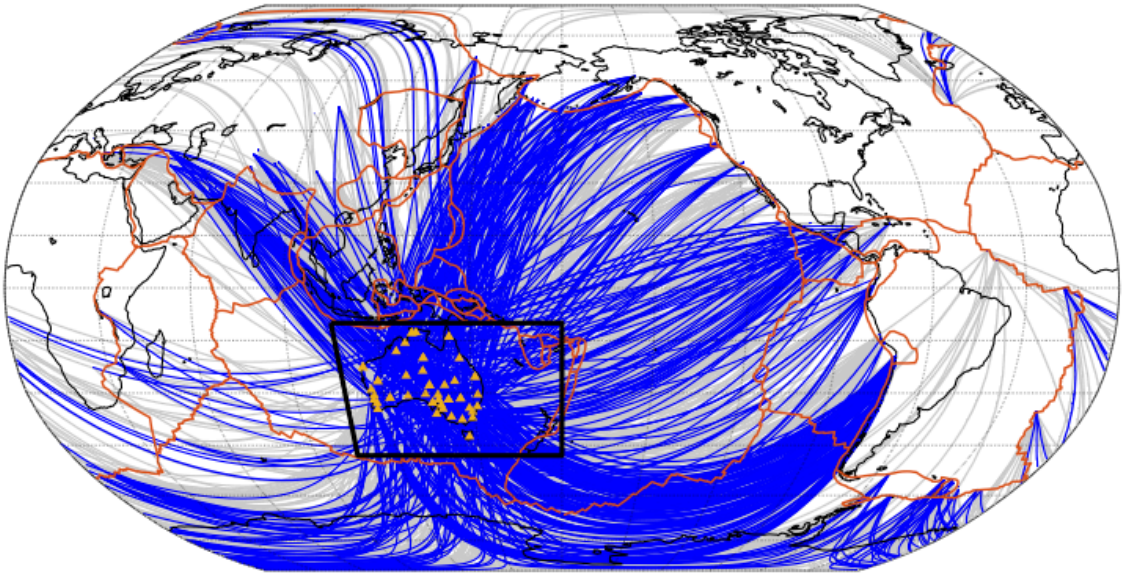

Figure 2. Global distribution of source-receiver paths analyzed for QL waves. Raypaths on which QL waves were present are shown in blue, the remainder in grey. The location of anisotropic gradients within the area of interest (black box, Figs. 3-4) is investigated using 43 seismic receivers (yellow triangles) based within Australia. Plate boundaries (in orange) from [31].

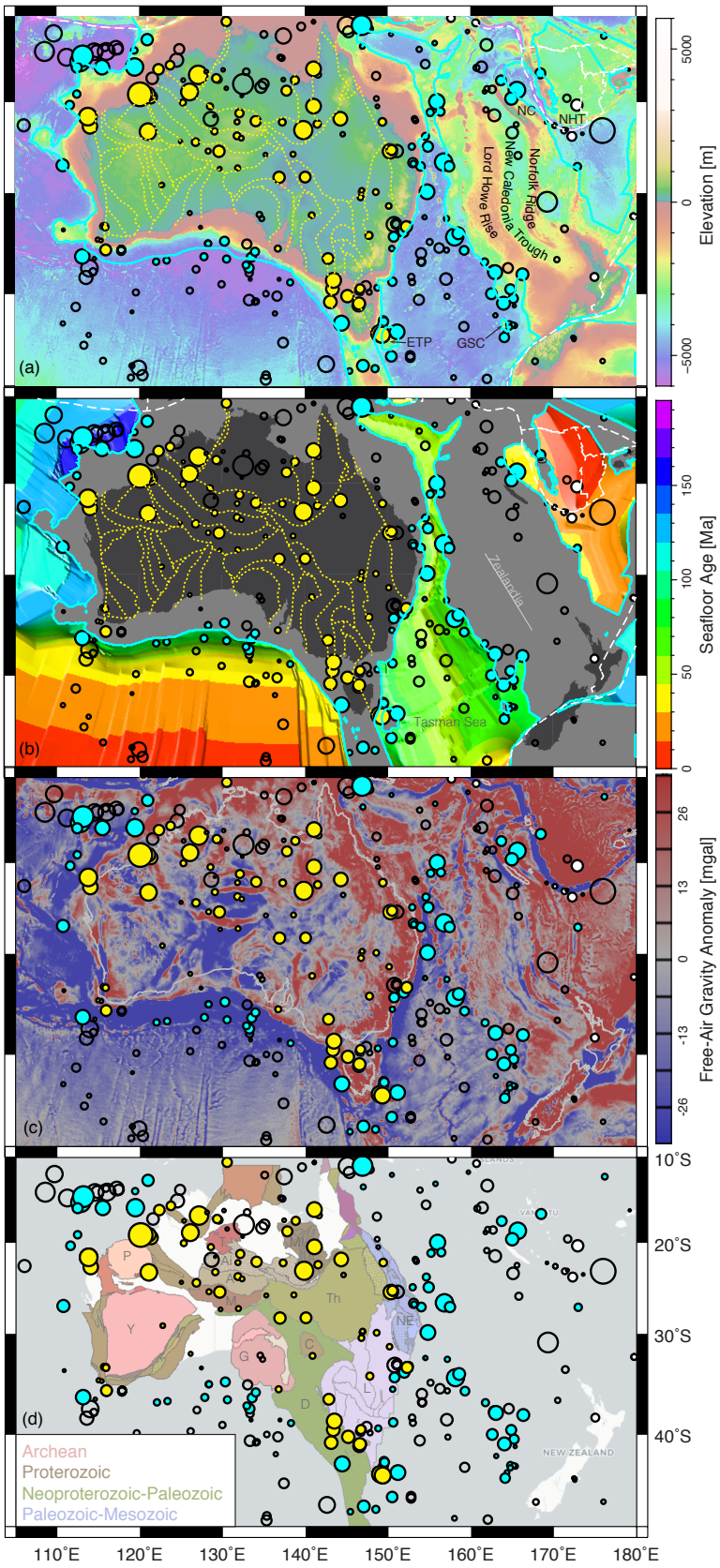
(a)
NC
NHT
Norfolk Ridge
New Caledonia Trough
Lord Howe Rise
ETP
GSC
Elevation [m]
5000
0
−5000
(b)
Zealandia
Tasman Sea
Seafloor Age [Ma]
150
100
50
0
(c)
Free-Air Gravity Anomaly [mgal]
26
13
0
-13
-26
(d)
Archean
Proterozoic
Neoproterozoic-Paleozoic
Paleozoic-Mesozoic
NEW ZEALAND
10˚S
20˚S
30˚S
40˚S
110˚E
120˚E
130˚E
140˚E
150˚E
160˚E
170˚E
180˚E

Figure 3. QL wave scattering points (black circles) compared to (a): surface topography [32], (b): continental versus oceanic crust and seafloor age [17], (c): free-air gravity [33], and (d): major tectonic provinces of Australia [34]. Circles are scaled in size relative to the amplitude of the QL wave. Those which coincide (within 1°) with either a plate boundary (dashed white lines), the ocean-continent margin (solid cyan lines), or major crustal boundaries within Australia (dotted yellow lines) [19], are highlighted by a solid circle with the respective color. In (a) abbreviations are as follows: ETP- East Tasman Plateau, GSC- Gilbert Seamount Complex, NC- New Caledonia, NHT- New Hebrides Trench. In (d) abbreviations refer to major tectonic provinces: A- Arunta, Ai- Aileron, C- Curnamona, D- Delamerian, G- Gawler, L- Lachlan, M- Musgrave, MI- Mount Isa, NE- New England, P- Pilbara, T- Tanami, Th- Thomson, Y- Yilgarn.

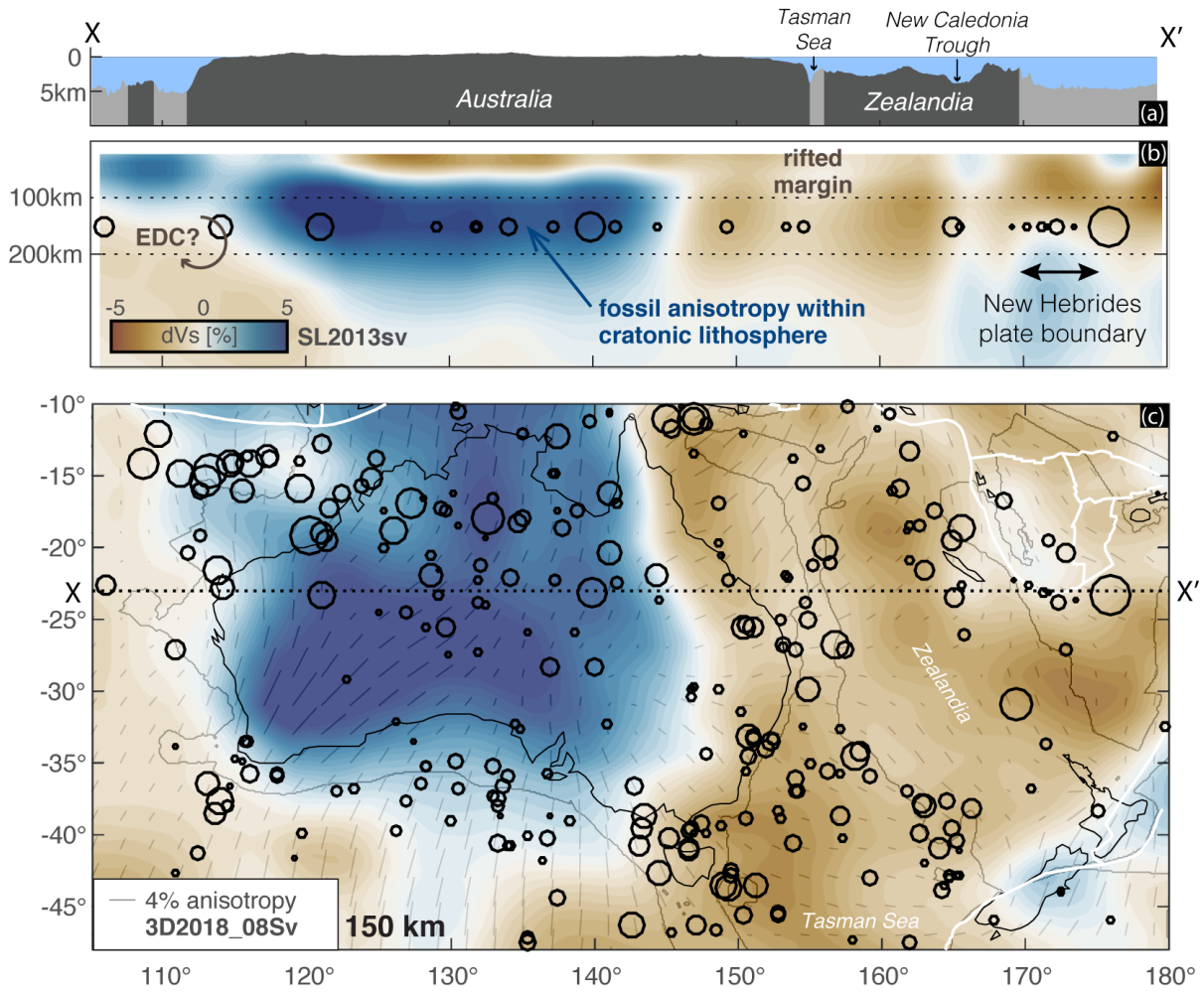

Figure 4. Interpretation of QL wave scatterers in relation to lithospheric versus asthenospheric mantle anisotropy. (a): Cross-section of elevation [32] along profile X-X', with dark versus light grey shading signifying continental versus oceanic crust. (b): Shear wave velocities from SL2013sv [35] along the same X-X' cross-section. Scatterers (black circles) are plotted at 150km depth, while dotted black lines represent zone of peak sensitivity from 100-200km. (c): Horizontal slice of SL2013sv velocity model at 150km depth, overlain by azimuthal anisotropy from 3D2018_08Sv [2]. Orientation and length of small grey bars correspond to the fast direction and strength (%) of azimuthal anisotropy. Thin continuous thin grey lines represent the continental margins, while white lines are plate boundaries (same as Fig. 3).